

Quantum Theory of Recollisional ($e, 2e$) Process in Strong Field Nonsequential Double Ionization of Helium

Zhangjin Chen,¹ Yaqui Liang,^{1,2} and C. D. Lin¹

¹*J. R. Macdonald Laboratory, Physics Department, Kansas State University, Manhattan, Kansas 66506-2604, USA*

²*College of Physics, Liaoning University, Shenyang 110036, People's Republic of China*

(Received 7 January 2010; revised manuscript received 7 February 2010; published 21 June 2010)

Based on the full quantal recollision model and field-free electron impact ionization theory, we calculate the correlated momentum spectra of the two outgoing electrons in strong field nonsequential double ionization (NSDI) of helium to compare with recent experiments. By analyzing the relative strength of binary versus recoil collisions exhibited in the photoelectron spectra, we confirm that the observed fingerlike structure in the experiment is a consequence of the Coulomb interaction between the two emitted electrons. Our result supports the recollision mechanism of strong field NSDI at the most fundamental level.

DOI: 10.1103/PhysRevLett.104.253201

PACS numbers: 34.50.Rk, 32.80.Fb, 32.80.Rm, 34.80.Dp

Nonsequential double ionization (NSDI) of atoms by intense linearly polarized laser fields has continued to draw considerable theoretical and experimental interest in the last two decades. Its attractiveness owes much to the fact that both the coupling between electrons with the laser field and the electron-electron interaction cannot be treated as perturbations. Qualitatively NSDI experiments are understood based on the semiclassical “recollision” model [1,2], where an electron first released from the atom by the laser field is driven back to recollide with the target ion and liberate another electron, in a process analogous to electron impact ionization, or the ($e, 2e$) process. Many experiments have been performed, from the total double ionization yield vs laser intensity [3], ion momentum distributions along the direction of laser polarization, to momentum correlation between the two outgoing electrons [4–9]. In the meantime, there is no shortage of efforts on the theory side. A complete theoretical understanding of NSDI should permit quantitative explanation of the measured two-electron momentum spectra. Such attempts include direct numerical solution of the two-electron time-dependent Schrödinger equation [10,11] and classical equation of motion [12]. These pure numerical calculations do not employ the rescattering concept directly. Calculations employing the rescattering concept include the S -matrix theory [13,14] where the ($e, 2e$) is solved by first-order perturbation, and semiclassical theory [15,16] where the ($e, 2e$) is calculated using classical mechanics. In this Letter we employ a full quantum formulation of the rescattering model and quantum scattering theories for the ($e, 2e$) process to calculate the momentum spectra of the two outgoing photoelectrons. Our aim is to interpret the experimental results reported in Staudte *et al.* [11] and in Rudenko *et al.* [17], where the two-electron momentum distributions along the laser polarization axis exhibit pronounced V -shaped, or fingerlike structure.

The starting point of our approach is the quantitative rescattering (QRS) theory [18] which has been applied to other rescattering processes such as high-order harmonic generation [19] and high-energy above-threshold ionization (HATI) electrons [20]. According to QRS, after the initial tunneling ionization, there will be an electron wave packet $W(k_r)$ that returns at time t_r to recollide with the target ion. We can obtain this wave packet from the HATI momentum spectra or from experiment [20]. By weighting the ($e, 2e$) differential cross sections with the returning electron momentum distribution $W(k_r)$, the yield for the emission of the two outgoing electrons can be calculated. However, in NSDI ionization occurs in the laser field. For ($e, 2e$) process that occurs at time t_r when the vector potential of the laser field is $\mathbf{A}(t_r) = \mathbf{A}_r$, after the collision,

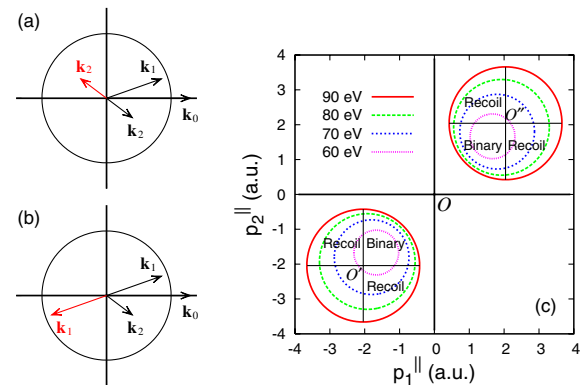


FIG. 1 (color online). (a) Schematic of laser-free ($e, 2e$) collisions. Index 1 for the scattered electron and 2 for the ejected electron. For electron 2, both the binary collisions (black arrow) and recoil collisions (red arrow) are indicated. (b) Same as (a) but electrons 1 and 2 are interchanged. (c) Kinematically allowed region of the momentum components parallel to the laser polarization axis for the two outgoing electrons in the recollisional ($e, 2e$) process.

each electron is still under the influence of the laser field. From t_r to the end of the laser pulse (where the vector potential is zero) each electron will gain an additional momentum $-A_r$ in the direction of laser polarization (atomic units are used). Thus, the measured photoelectron momentum is given by

$$p^{\parallel} = -A_r + k_r^{\parallel}, \quad p^{\perp} = k_r^{\perp}, \quad (1)$$

or $\mathbf{p} = -\mathbf{A}_r + \mathbf{k}_r$. According to the QRS, it was further established that $k_r = 1.26|A_r|$. Note that for each optical cycle, as the laser field oscillates there are two wave packets returning to the target ion, one from the “right” and another from the “left.” We will consider long pulses where the left and right wave packets are equivalent.

We first analyze the constraints on the momenta for the field-free ($e, 2e$) process. Let $\mathbf{k}_r = \mathbf{k}_0$, where \mathbf{k}_0 is the momentum of the incident electron. After collision, we use \mathbf{k}_1 for the momentum of the scattered particle and \mathbf{k}_2 for the ejected particle. Figure 1(a) depicts such a collision. For a given \mathbf{k}_0 , when \mathbf{k}_1 is fixed, it is known from ($e, 2e$) that there are two favored scattering angles for \mathbf{k}_2 . The first one is called binary collision, where $k_2^{\perp} = k_1^{\perp}$. The second one is called recoil collision where electron 2 is ejected after it is further backscattered from the nucleus. As illustrated in Fig. 1(a), for binary collisions ($k_1^{\parallel} > 0, k_2^{\parallel} > 0$) and for recoil collisions ($k_1^{\parallel} > 0, k_2^{\parallel} < 0$). Since the two outgoing electrons are indistinguishable, an exchange effect should be considered. In Fig. 1(b) we consider \mathbf{k}_2 for the scattered electron and \mathbf{k}_1 for the ejected electron. The binary peak and the recoil peak are also shown.

In all two-electron momentum measurements, only the momentum component of each electron along the polarization axis has been reported. For each incident energy $E_0 = k_0^2/2$, energy conservation requires $E_0 - I_p = k_1^2/2 + k_2^2/2$ where $I_p = 54.4$ eV is the ionization potential of He^+ . In Fig. 1(c), we depict the bound of $(k_1^{\parallel}, k_2^{\parallel})$ in a 2D plot of $(p_1^{\parallel}, p_2^{\parallel})$ for each value of E_0 . The ($e, 2e$) collisions depicted in Figs. 1(a) and 1(b) have spectra located in the third quadrant. For “incident” electrons from the opposite direction, the spectra are located in the first quadrant. The center of each circle is shifted from the origin by an amount $|A_r|$ along each axis and the circle shrinks to a point at the ionization threshold. In Fig. 1(c), for the highest incident energy, we further indicate the regions for the binary collisions and recoil collisions, respectively. This analysis relates the phase space of the momenta of the two outgoing electrons measured in the laboratory to the contributions of binary collisions vs recoil collisions in the laser field.

We next show in Fig. 2(a) the experimental correlated momentum spectra from Staudte *et al.* [11]. It shows that there are counts covering regions in $(p_1^{\parallel}, p_2^{\parallel})$ that are not allowed in Fig. 1(c), in particular, in the second and fourth quadrants. These events are due to indirect processes in

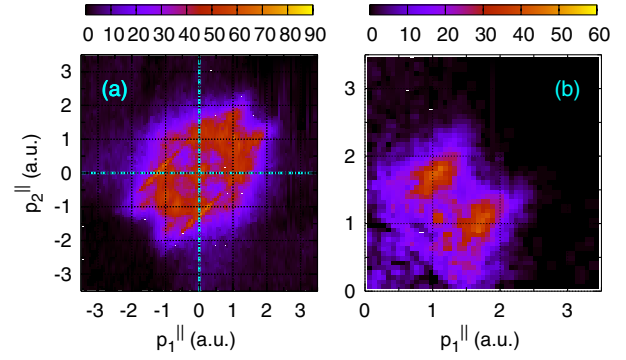


FIG. 2 (color online). (a) Experimental correlated momentum spectra along the polarization direction for double ionization of helium at 800 nm, 4.5×10^{14} W/cm². (b) Same as (a) in the first quadrant, only the ($e, 2e$) portion is retained, see text. The original data are from Staudte *et al.* [11].

NSDI where an electron in the target ion is first excited by the returning electron, followed by tunneling ionization of the excited electron by the laser. These excitation-tunneling events are symmetric with respect to the two momentum axes [9]. Using the original data of [11], we take the average of the corresponding data points in the second and fourth quadrants. By subtracting this average from the corresponding data points in the first quadrant, we obtain the true experimental correlated momentum spectra from the direct ($e, 2e$) processes. The results are shown in Fig. 2(b). An identical true ($e, 2e$) spectra is obtained for the third quadrant.

After having analyzed the kinematics of the two outgoing electrons, we next employ the laser-free ($e, 2e$) scattering theory to calculate the differential cross sections and use Fig. 1(c) to translate the results to compare with the measured photoelectron spectra.

The laser-free ($e, 2e$) scattering amplitude is given by

$$f(\mathbf{k}_1, \mathbf{k}_2) = \langle \Psi_{\mathbf{k}_1, \mathbf{k}_2}^- | V_i | \Psi_{\mathbf{k}_0} \rangle. \quad (2)$$

The final-state wave function $\Psi_{\mathbf{k}_1, \mathbf{k}_2}^-$ for two continuum electrons in the potential from the nucleus should be the “exact” solution of the two-electron Hamiltonian with the incoming wave boundary condition. Since no exact solutions are available, various approximations will be used below. Based on Eq. (2), clearly the two-electron momentum correlation spectra in ($e, 2e$) depend most sensitively on the final-state wave function $\Psi_{\mathbf{k}_1, \mathbf{k}_2}^-$. A commonly used approximate wave function in ($e, 2e$) for two electrons in the continuum is the so-called BBK model of Brauner, Briggs, and Klar [21]

$$\begin{aligned} \Psi_{\mathbf{k}_1, \mathbf{k}_2}^-(\mathbf{r}_1, \mathbf{r}_2) &= (2\pi)^{-3} \exp(i\mathbf{k}_1 \cdot \mathbf{r}_1) \exp(i\mathbf{k}_2 \cdot \mathbf{r}_2) \\ &\quad \times C(\alpha_1, \mathbf{k}_1, \mathbf{r}_1) C(\alpha_1, \mathbf{k}_2, \mathbf{r}_2) \\ &\quad \times C(\alpha_{12}, \mathbf{k}_{12}, \mathbf{r}_{12}), \end{aligned} \quad (3)$$

where the Coulomb function is

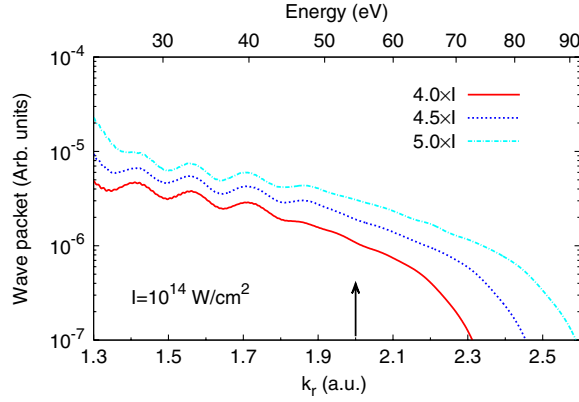


FIG. 3 (color online). Wave packets against the momentum of the recolliding electron (the bottom horizontal axis) for 15 fs (FWHM) laser pulses at peak intensities of 4.0, 4.5, and 5.0×10^{14} W/cm² with wavelength of 800 nm. The arrow indicates the minimum momentum of the recolliding electron to ionize the parent ion He⁺. The returning electron energy is marked on the top horizontal axis.

$$C(\alpha, \mathbf{k}, \mathbf{r}) = \exp(-\pi\alpha/2)\Gamma(1-i\alpha) \times {}_1F_1[i\alpha; 1; -i(kr + \mathbf{k} \cdot \mathbf{r})] \quad (4)$$

and

$$\mathbf{k}_{12} = (\mathbf{k}_1 - \mathbf{k}_2)/2, \quad \mathbf{r}_{12} = \mathbf{r}_1 - \mathbf{r}_2, \\ \alpha_1 = -Z_N/k_1, \quad \alpha_2 = -Z_N/k_2, \quad \alpha_{12} = 1/2k_{12}. \quad (5)$$

Equation (3) is a product of Coulomb functions between each pair of charged particles. The perturbation V_i in Eq. (2) is

$$V_i = 1/r_{12} - Z_N/r_1 - U_i(r_1), \quad (6)$$

where $Z_N = 2$ is the charge of the nucleus.

The initial two-electron wave function is taken to be

$$\Psi_{\mathbf{k}_0}(\mathbf{r}_1, \mathbf{r}_2) = \varphi_{\mathbf{k}_0}(\mathbf{r}_1)\phi_{\text{He}^+}(\mathbf{r}_2), \quad (7)$$

where $\varphi_{\mathbf{k}_0}(\mathbf{r}_1)$ describes the incident electron in potential $U_i(r)$ and $\phi_{\text{He}^+}(\mathbf{r}_2)$ is the ground state wave function of He⁺. For the initial state, if we set $U_i(r) = 0$ for the incident electron, then $U_i(r) = 0$ is a plane wave. We will use P-CCC to denote transition amplitudes calculated with the incident electron described by a plane wave and the final-state wave function given by the BBK, since in BBK the final-state wave function is the product of three Coulomb functions. Note that one can drop the last C function in Eq. (3) by setting $\alpha_{12} = 0$ in Eq. (5). This represents that electron-electron repulsion between the two electrons in the final state has been neglected. We use P-CC to denote this approximation.

To account for the fact that the two electrons are indistinguishable, the triple differential cross section (TDCS) for electron impact ionization process is given by

$$\frac{d^3\sigma}{d\Omega_1 d\Omega_2 dE} = (2\pi)^4 \frac{k_1 k_2}{k_0} \left[\frac{3}{4} |f(\mathbf{k}_1, \mathbf{k}_2) - g(\mathbf{k}_1, \mathbf{k}_2)|^2 + \frac{1}{4} |f(\mathbf{k}_1, \mathbf{k}_2) + g(\mathbf{k}_1, \mathbf{k}_2)|^2 \right], \quad (8)$$

where $\Omega_1(\theta_1, \phi_1)$ and $\Omega_2(\theta_2, \phi_2)$ are the solid angles of \mathbf{k}_1 and \mathbf{k}_2 , and $g(\mathbf{k}_1, \mathbf{k}_2)$ is the exchange amplitude with $g(\mathbf{k}_1, \mathbf{k}_2) = f(\mathbf{k}_2, \mathbf{k}_1)$. Finally, to compare with experimental measurements for a given incident energy E_0 , we have to integrate the TDCS over unobserved degrees of freedom,

$$Y_{E_0}(k_1^{\parallel}, k_2^{\parallel}) = \frac{1}{k_1 k_2} \int_0^{E_{\max}} dE_2 \int_0^{2\pi} d\phi_2 \frac{d^3\sigma}{d\Omega_1 d\Omega_2 dE_2} \Big|_{\phi_1=0}, \quad (9)$$

where $E_{\max} = E_0 - I_p$. In Eq. (9), we set $\phi_1 = 0$ due to the cylindrical symmetry.

To generate correlated parallel electron momentum spectra from NSDI to compare with experimental data, two more levels of integration have to be carried out. First, in a laser experiment, the returning energy of the wave packet for each peak intensity has a distribution $W(k_r)$. Second, peak laser intensity is not uniform within the laser focus volume from which the electrons are collected. As shown elsewhere [20], using the QRS, the result of including volume integration is to replace $W(k_r)$ by a volume integrated wave packet $W_V(I_0, k_r)$ which depends on the peak intensity I_0 at the laser focus. In Fig. 3 we show $W_V(I_0, k_r)$ for three peak intensities at $I_0 = 4.0, 4.5,$ and 5.0×10^{14} W/cm². The arrow indicates the minimum returning electron momentum needed for ($e, 2e$) to be energetically possible. In Figs. 4(a) and 4(b) we show the calculated parallel momentum distributions using the P-CC and P-CCC models, respectively, for laser intensity of 4.5×10^{14} W/cm² from Staudte *et al.* [11]. (Only the first quadrant is shown since the spectra in the third quadrant can be obtained by inversion.) Comparing to Fig. 2(b), it clearly shows that the P-CCC predictions are much closer to the experimental data while the P-CC model fails completely.

Despite of its success, the P-CCC still is a very simple theory. The maximum returning energy of the electron in the measurement is only 31 eV above the ionization threshold. For such low energy collisions, the P-CCC model is not expected to be very accurate. First, the interaction between two charged particles in BBK is not screened by the presence of the third charge; thus, Coulomb repulsion between the two electrons is too large and the recoil peak is overemphasized. This deficiency is corrected by introducing an effective Sommerfeld parameter for each pair of charges [22]. Such modifications incorporate dynamic screening (DS) among the three pairs of Coulomb interactions and hence are called DS3C. The spectra of DS3C are shown in Fig. 4(d). Compared to P-CCC model, one can see an increase of the yield in the binary collision

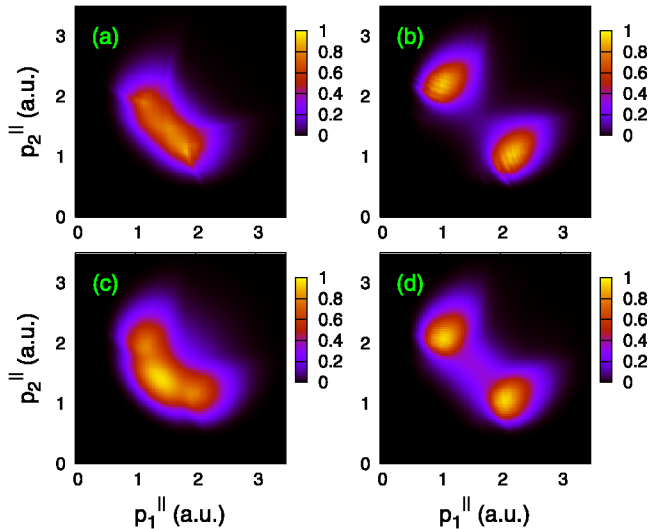


FIG. 4 (color online). Momentum spectra of the two outgoing electrons in the recollisional ($e, 2e$) process on He^+ at 800 nm, and peak intensity of $4.5 \times 10^{14} \text{ W/cm}^2$ at the laser focus. Shown are the momentum components along the polarization axis for each electron. The theoretical models used are (a) P-CC, (b) P-CCC, (c) C-CC, and (d) DS3C, respectively.

region and thus in better agreement with Fig. 2(b). Another improvement is to use Coulomb wave for the incident electron. Using Coulomb waves, however, the scattering amplitude can only be conveniently calculated for the C-CC model. The results from the C-CC model are shown in Fig. 4(c). Comparing to Fig. 4(a), the binary peak is enhanced with the use of incident Coulomb waves. Generalizing from this, we anticipate that replacing plane wave by Coulomb wave for the initial state but using DS3C for the final state would give a stronger binary peak and a weaker recoil peak than in Fig. 4(d). Based on these results, we can conclude that electron-electron interaction between the two electrons is responsible for the appearance of a fingerlike structure in the correlated momentum correlation.

There are other more advanced ($e, 2e$) theories that have been applied to electron impact ionization of neutral atoms. These include the convergent close coupling theory [23], R -matrix theory [24], the exterior complex scaling method [25], and the direct integration of the time-dependent Schrödinger equation method [26]. These calculations are rather time consuming but can be carried out. Using the QRS model, these ($e, 2e$) theories can be used to obtain more accurate two-electron momentum spectra for the NSDI processes.

We comment that not every NSDI experiment need be interpreted with sophisticated ($e, 2e$) collision theories. For example, we found that longitudinal ion momentum distributions calculated using P-CC and P-CCC are nearly identical in shape. Such ion momentum distributions depend more critically on the returning electron momentum

distributions. Thus for short pulses they are sensitive to the carrier-envelope phase of the laser [27].

In summary, we demonstrated that the fingerlike structure in the correlated two-electron momentum spectra observed in the recent nonsequential double ionization of helium [11,17] can be quantitatively predicted based on a full quantum mechanical recollision model and field-free ($e, 2e$) collision theory. Coulomb repulsion between the two outgoing electrons has been found to be responsible for the observed fingerlike structure. These results support the interpretation of recollision mechanism for strong field nonsequential double ionization of atoms at the most basic level.

We thank Dr. A. Staudte for providing data in digital form that allowed us to plot Fig. 2. This work was supported in part by Chemical Sciences, Geosciences and Biosciences Division, Office of Basic Energy Sciences, Office of Science, U.S. Department of Energy.

-
- [1] P. B. Corkum, *Phys. Rev. Lett.* **71**, 1994 (1993).
 - [2] J. L. Krause, K. J. Schafer, and K. C. Kulander, *Phys. Rev. Lett.* **68**, 3535 (1992).
 - [3] B. Walker *et al.*, *Phys. Rev. A* **48**, R894 (1993).
 - [4] E. Eremina *et al.*, *J. Phys. B* **36**, 3269 (2003).
 - [5] R. Moshhammer *et al.*, *J. Phys. B* **36**, L113 (2003).
 - [6] A. S. Alnaser *et al.*, *J. Phys. B* **41**, 031001 (2008).
 - [7] Th. Weber *et al.*, *Nature (London)* **405**, 658 (2000).
 - [8] M. Weckenbrock *et al.*, *Phys. Rev. Lett.* **92**, 213002 (2004).
 - [9] B. Feuerstein *et al.*, *Phys. Rev. Lett.* **87**, 043003 (2001).
 - [10] J. S. Parker *et al.*, *Phys. Rev. Lett.* **96**, 133001 (2006).
 - [11] A. Staudte *et al.*, *Phys. Rev. Lett.* **99**, 263002 (2007).
 - [12] S. L. Haan *et al.*, *J. Phys. B* **42**, 134009 (2009).
 - [13] A. Becker and F. H. M. Faisal, *Phys. Rev. Lett.* **89**, 193003 (2002).
 - [14] C. Figueira de Morisson Faria *et al.*, *Phys. Rev. A* **69**, 043405 (2004).
 - [15] A. Emmanouilidou, *Phys. Rev. A* **78**, 023411 (2008).
 - [16] D. F. Ye, X. Liu, and J. Liu, *Phys. Rev. Lett.* **101**, 233003 (2008).
 - [17] A. Rudenko *et al.*, *Phys. Rev. Lett.* **99**, 263003 (2007).
 - [18] T. Morishita *et al.*, *Phys. Rev. Lett.* **100**, 013903 (2008).
 - [19] A. T. Le *et al.*, *Phys. Rev. A* **80**, 013401 (2009).
 - [20] Z. Chen *et al.*, *Phys. Rev. A* **79**, 033409 (2009).
 - [21] M. Brauner, J. S. Briggs, and H. Klar, *J. Phys. B* **22**, 2265 (1989).
 - [22] Z. Chen *et al.*, *Phys. Rev. A* **56**, R2514 (1997).
 - [23] I. Bray *et al.*, *J. Phys. B* **35**, R117 (2002).
 - [24] P. G. Burke and K. A. Berrington, *Atomic and Molecular Processes: An R-Matrix Approach* (Institute of Physics Publishing, Bristol, 1993).
 - [25] C. W. McCurdy, M. Baertschy, and T. N. Rescigno, *J. Phys. B* **37**, R137 (2004).
 - [26] M. S. Pindzola *et al.*, *J. Phys. B* **40**, R39 (2007).
 - [27] X. Liu *et al.*, *Phys. Rev. Lett.* **93**, 263001 (2004).